Biosensors and Bioelectronics 127 (2019) 194–199

Contents lists available at ScienceDirect

Biosensors and Bioelectronics

journal homepage: www.elsevier.com/locate/bios

An electrochemical sensor for Oct4 detection in human tissue based on target-induced steric hindrance effect on a tetrahedral DNA nanostructure

Jiehua Ma[a,b], Lan Xue[a], Meiling Zhang[c], Chao Li[a], Yang Xiang[a], Ping Liu[c,*], Genxi Li[a,d,**]

[a] State Key Laboratory of Pharmaceutical Biotechnology and Collaborative Innovation Center of Chemistry for Life Sciences, Department of Biochemistry, Nanjing University, Nanjing 210093, PR China
[b] State Key Laboratory of Reproductive Medicine, Department of Reproductive Health, Obstetrics and Gynecology Hospital Affiliated to Nanjing Medical University, Nanjing 210004, PR China
[c] Department of Oncology, the First Affiliated Hospital of Nanjing Medical University, Nanjing 210029, PR China
[d] Center for Molecular Recognition and Biosensing, School of Life Sciences, Shanghai University, Shanghai 200444, PR China

ARTICLE INFO

Keywords:
Electrochemical sensor
Steric hindrance effect
Oct4
Tetrahedral DNA nanostructure
Human tissue sample

ABSTRACT

Here, we report an electrochemical sensor for rapid and sensitive detection of octamer-binding transcription factor 4 (Oct4) in human tissue samples by utilizing a designed tetrahedral DNA nanostructure (TDN). In the design, the TDN is also extended with two additional strands from two vertices. When Oct4 is absent, the strands are linked together by complementary pairing bases. Owing to the rigid structure of TDN, contact of the redox labels on the signal strand and electrode surface is greatly prohibited, resulting in a lower electrochemical signal. However, the specific binding of Oct4 to the edge of the tetrahedron will liberate the signal strand and increase the redox current dramatically. Experimental results reveal that the proposed sensor shows a linear range of 0.5–1000 ng/mL with a detection limit of 60 pg/mL. Moreover, it can be directly applied to clinical sample detection. This sensor can also achieve one-step detection of Oct4 in less than 30 min. Furthermore, through replacing the binding site, this sensor can be easily extended to a wide application range of DNA binding proteins.

1. Introduction

Malignant tumor is a kind of disease that seriously endangers human health and life. Although the technology of medical diagnosis and treatment has been greatly improved, the overall mortality and survival rate of the tumor patients have not been improved significantly. Recurrence and metastasis are still the main causes of poor prognosis of cancer. In recent years, a few cells with potential of self-renewal, proliferation and differentiation have been found and named as cancer stem cells, which may be the basis of tumor growth, reproduction and the ultimate cause of recurrence and metastasis. Octamer-binding transcription factor 4 (Oct4) has been implicated as a marker of cancer stem cells (Atlasi et al., 2007; Kim and Nam, 2011), which was previously known as the gatekeeper of pluripotent embryonic state (Looijenga et al., 2003). It is over-expressed in a variety of cancers including ovarian cancer (Comisso et al., 2017; Zhao et al., 2018), cervical cancer (Kim et al., 2015; Shen et al., 2014; Wang et al., 2013; Yan et al., 2016), lung cancer (Li et al., 2016), pancreatic cancer (Lu et al., 2013) and esophageal cancer (Ge et al., 2010). Elevated Oct4 level is frequently correlated with the clinicopathological features, metastasis and poor clinical outcomes in cancers of various origins (Kar and Patra, 2018; Yin et al., 2012; Zhao et al., 2016). As a consequence, the detection of Oct4 protein is critical for the tumor prognostic evaluation and efficacy monitoring of drug intervention.

The currently available methods for Oct4 protein assay, such as Western blotting and ELISA, are expensive, cumbersome and time-consuming. A few efforts have been devoted to overcoming these shortcomings (Ma et al., 2018; Sharma et al., 2017). We once explored an alternative strategy for Oct4 detection based on anti-dsDNA antibody-decorated Fe_3O_4 magnetite nanoparticles (Ma et al., 2018). However, the method still depends on the expensive antibody and fluorescent instruments and has not been applied to the detection of clinical samples. Therefore, a cost-effective, simple and rapid method for measuring Oct4 in real samples is highly required. Electrochemical technique may offer an alternative tool due to the characteristics that they are simple, sensitive, and inexpensive (Nie et al., 2007; Zhang

* Corresponding author.
** Corresponding author at: State Key Laboratory of Pharmaceutical Biotechnology and Collaborative Innovation Center of Chemistry for Life Sciences, Department of Biochemistry, Nanjing University, Nanjing 210093, PR China.
E-mail addresses: liupinga288@163.com (P. Liu), genxili@nju.edu.cn (G. Li).

https://doi.org/10.1016/j.bios.2018.12.029
Received 12 September 2018; Received in revised form 3 December 2018; Accepted 15 December 2018
Available online 21 December 2018
0956-5663/

et al., 2005). On the other hand, tetrahedral DNA nanostructure (TDN) has gradually become the research focus in the field of sensor (Ge et al., 2018; Li et al., 2018a; Ozhalici-Unal and Armitage, 2009). Compared with single-stranded DNA (ssDNA) or DNA hairpins-based electrochemical DNA (E-DNA), TDN offers many advantages, such as high capture capability, low background current, and better stability and insensitivity in complex samples (Kim et al., 2013; Yang et al., 2018). Thus, TDN-based biosensors for various analytes have been developed, such as nucleic acids, proteins and small molecules.

Steric hindrance effect is an effective signal transduction mode, which has been used in a few analytical methods of biological molecules. For example, we have proposed an electrochemical method based on steric hindrance effect-induced resolution of an electrode-bound DNA pseudoknot (Ma et al., 2016). Thanks to the relatively rigid structure of DNA pseudoknot and already existing binding site, the method achieved low backgrounds and effective thermodynamics. Nevertheless, the method failed to meet the needs of complex clinical samples, such as human tumor tissue due to insufficient stability of the probe. Li and co-workers (Li et al., 2018b) have reported a fluorescent assay based on steric hindrance caused by a sandwich-like ternary complex, which is formed by the target and its split aptamers. However, cleavage aptamers may decrease the affinity between the target and its split aptamers. Therefore, we believe that the introduction of steric hindrance into TDN-based sensors can solve these problems and improve analytical performance, especially in complex samples. Herein, we have fabricated an electrochemical sensor for Oct4 detection based on target-induced steric hindrance effect on a TDN.

To do so, a TDN with two additional strands attached to two vertices is designed (Scheme 1). Specially, the top stand acts as assistant strand (strand a) and the other one at the bottom functions as signal strand (strand b). Table S1 shows the sequence information for each strand of the TDN that we have designed. The putative binding site of Oct4 (5′-ATT TGC AT-3′)(Li et al., 2014) and its complementary sequence (5′-AT GCA AAT-3′) are designed in two strands. When a TDN forms, these two complementary chains will appear on the edge of the tetrahedron, which allows specific binding of Oct4 to the tetrahedron. When the target is absent, the strands a and b are linked together by complementary pairing bases. Owing to the rigid structure of TDN, the contact between redox label and underlying gold electrode is reduced, and the background current can be minimized. However, in the presence of the target, the Oct4 binding to the tetrahedron will interrupt the hybridization between the strand a and strand b, due to the relatively large size of the resulting DNA and Oct4 complex (5.37 × 6.95 × 8.45 nm), which causes large steric hindrance effect. As a result, the signaling element of strand b will be liberated to the electrode surface and greatly increase redox current.

2. Experimental section

2.1. Materials and reagents

DNA oligonucleotides used in this work were synthesized and purified by Sangon Biotechnology Co. Ltd. (Shanghai, China). Bovine serum albumin (BSA) and Tris (2-carboxyethyl)phosphine hydrochloride (TCEP) were obtained from Sigma-Aldrich (Shanghai, China). Recombinant human octamer binding transcription factor 4 (Oct4) protein was obtained from Abcam (Shanghai, China). All other chemicals not mentioned here were of analytical reagent grade.

The buffer solutions used in this work are listed as follows. TM buffer (10 mM Tris-HCl, pH 7.4, 10 mM $MgCl_2$) was the DNA tetrahedron preparation and immobilization buffer. Reaction buffer: 10 mM Tris-HCl (pH 7.4) with 0.3 M NaCl. Sample dilution buffer: 10 mM Tris–HCl, 140 mM NaCl, 1 mM $MgCl_2$, and 5 mM KCl, 1.0% Tween 20. Buffer for electrochemical detection of methylene blue (MB): 20 mM PBS, 0.5 M NaCl, pH 7.4. Buffer for electrochemical impedance spectroscopy (EIS): 5 mM $[Fe(CN)6]^{3-/4-}$ with 1 M KNO_3. All of the solutions were prepared with Milli-Q water from a Millipore system.

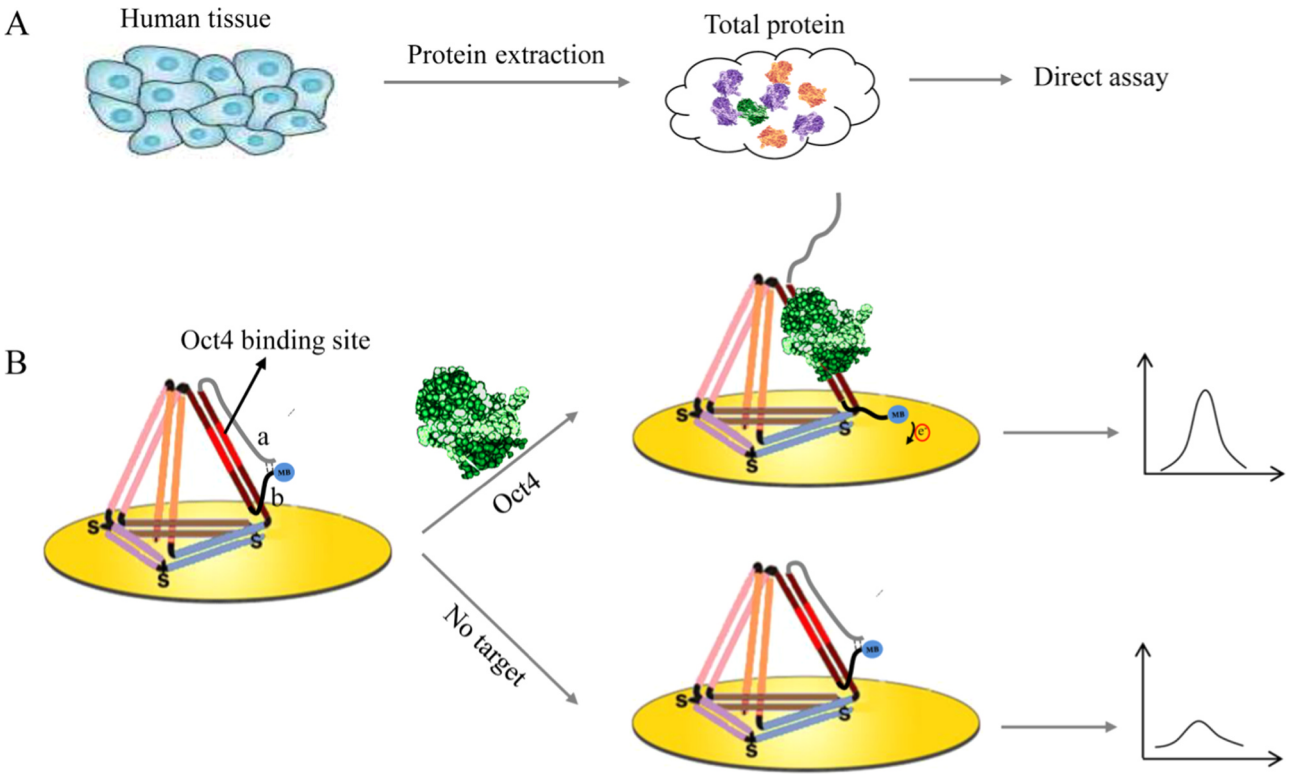

Scheme 1. Schematic illustration of the proposed sensor for Oct4 assay.

2.2. Preparation of TDN

To prepare TDN, four designed strands for the formation of the tetrahedrons were mixed in equimolar ratio in TM buffer. The solution was heated to 95 °C for 10 min and then quickly cooled to 4 °C. Atomic force microscopy (AFM) and gel electrophoresis were used for characterization of the synthesized TDN.

2.3. Electrode modification

2 mm in diameter Gold electrodes were immerged in piranha solution (H_2SO_4: 30% H_2O_2 = 3:1) for 15 min followed by rinsing with distilled water. Then, the electrodes were polished on a microcloth with 1 μm and 0.3 μm γ-alumina. After that, the electrodes were sonicated in distilled and ethanol water for 5 min each. Finally, the electrodes were electrochemically cleaned with 0.5 M H_2SO_4 (−0.35 V and 1.5 V). The above clean gold electrode was incubated with TDN for 1.5 h at RT. The concentration of TDN is 0.5 μM, which is diluted with buffer containing 5 mM TCEP. Between each step, the electrode was washed with double-distilled water and dried with N_2.

2.4. Detection of Oct4

Recombinant human Oct4 was first diluted with sample dilution buffer to different concentrations. The above prepared electrodes were treated with protein solutions for 20 min at 37 °C. Then, the electrodes were washed with buffer and used for electrochemical measurements. For the detection of Oct4 in human tissue, the samples were received from Obstetrics and Gynecology Hospital Affiliated to Nanjing Medical University between July 2018 and June 2017, which is approved by the Ethics Committee of Nanjing Maternal and Child Health Hospital. Ovarian tissue samples were collected from 10 patients with ovarian cancer and 10 control patients with benign ovarian disease. Cervical tissue was obtained from cancer tissues and adjacent tissues of 10 patients with cervical cancer. Tissue samples were immediately put into liquid nitrogen for 1 h and then transferred to −80 °C fridge for analysis experiments. Total proteins of tissue samples were extracted by RIPA Lysis Buffer according to the manufacturer's operation instructions and directly used for the analysis.

2.5. Electrochemical measurements

A three-electrode configuration involved a gold working electrode, a saturated calomel reference electrode (SCE) and a platinum wire counter electrode was employed in all of the experiments. All of the electrochemical measurements were carried out with a CHI 660D electrochemical workstation (CH Instruments Inc., Austin). The experimental parameters were as follows. SWVs: scan range, − 0.6 to − 0.1 V; step potential, 1 mV; frequency, 20 Hz; amplitude, 50 mV. EIS: bias potential, 0.225 V; frequency range, 0.1–10 kHz; amplitude, 5 mV.

3. Results and discussion

3.1. Validation of sensing mechanism

In order to characterize the stepwise modification and treatment of the electrode, Electrochemical impedance spectra (EIS) are recorded in $[Fe(CN)_6]^{3-/4-}$ electrolyte. As shown in Fig. 1, the EIS of bare gold electrode is similar to a straight line (curve a). However, after the immobilization of TDN, a large semicircle can be observed (curve b), indicating an increase of the electron transfer resistance, due to the reason that the negatively charged TDN on the electrode will electrostatically repel the also negative electroactive species $Fe(CN)_6^{3-/4-}$. Furthermore, after treatment with Oct4 protein, the electrochemical impedance dramatically increases (curve c), indicating the Oct4 binding with the TDN. Therefore, the step-by-step modification of the electrode surface has been confirmed and the binding between Oct4 and the TDN were proved by EIS.

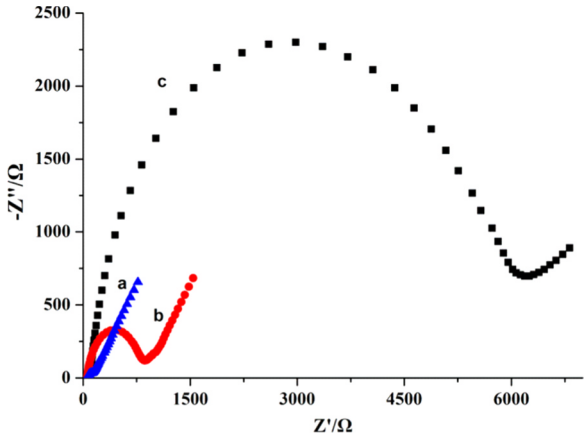

Fig. 1. Nyquist diagrams corresponding to the gold electrode at different modification stages. Curve (a) is for the bare gold electrode, while curves (b) and (c) are the cases after TDN modification, and further treatment with Oct4. Biasing potential: 0.224 V. Amplitude: 5 mV. Frequency range: 0.1 Hz–10 kHz.

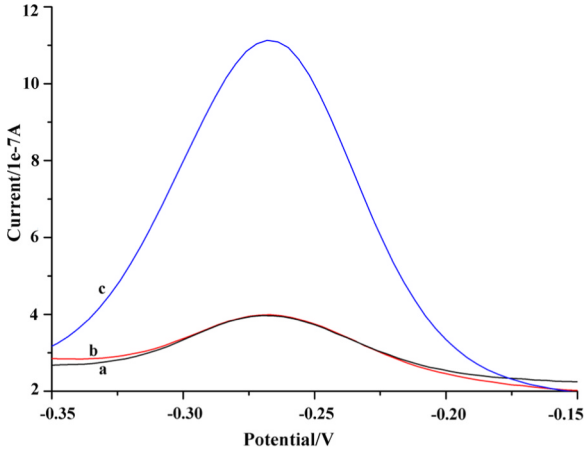

Fig. 2. SWVs obtained up analyzing the cases (a) in the absence of Oct4 binding sequence, (b) blank, (c) 500 ng/mL Oct4.

To investigate the feasibility of this sensor, the square wave voltammograms (SWV) are recorded upon different conditions (Fig. 2). In the absence of Oct4 binding sequence (Fig. 2a) or in the blank group (Fig. 2b), only small peaks can be detected. Nonsense strand was used to simulate deletion of binding sites. The blank control only contains Tris–HCl solution. The reason for the low signal is clear. Without binding of Oct4, the strands a and b are linked together and the electron communication of MB with the electrode does not occur. However, in the presence of Oct4, a significant current signal is observed, due to the separation of strand a and b caused by steric hindrance effect (Fig. 2c). The above results indicate the feasibility of our method for detection of Oct4.

3.2. Optimization of experimental conditions

Next, to achieve better analytical performance, we have optimized various experimental conditions. First of all, we have carefully optimized the spacer length of strand a. If strand a is too short or too long, a large background signal can be observed, as the MB head of strand b is free to get to the electrode and enhance electron transfer. The optimal length to form a tight loop has been estimated to be poly-9T for the spacer of strand (a-9T) (Table S1) according to the maximum length of

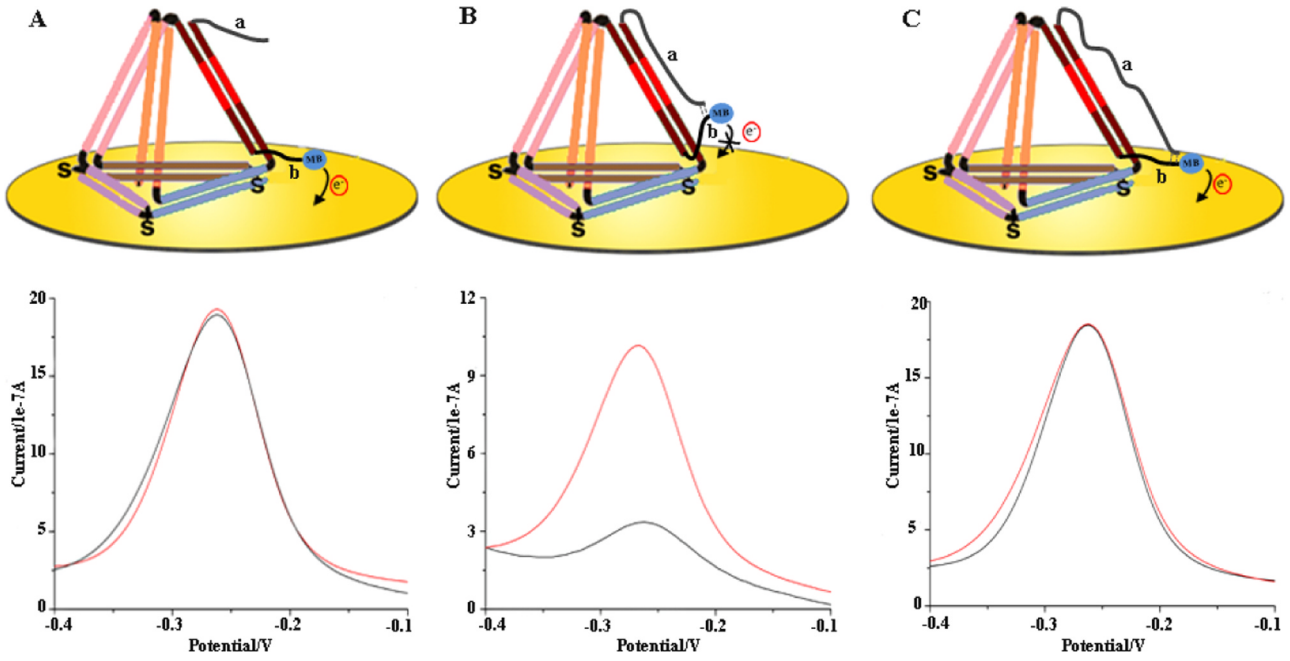

Fig. 3. Optimization of the spacer length of strand a for better analytical performance in the absence (black) or presence (red) of target (500 ng/mL): (A) a -3T, (B) a -9T, (C) a -12T.

nucleotide extension (0.5 nm per nucleotide). To validate the optimal length, we used poly-3T (a-3T) and poly-12T (a-12T) TDN modified electrode for the comparison. The result verifies our expectation that a-9 T TDN can efficiently get high signal and low background (Fig. 3). Secondly, 37 °C is proved to be the best reaction temperature, and the buffer with a pH of 7.4 for 30 min is favorable reaction interaction conditions (Fig. S2). So, we adopted these optimum reaction conditions in the following experiments. Finally, the experimental optimization was done for the fabrication of self-assembled monolayers (SAMs). We have optimized the surface density of the TDN by changing the concentration of TDN solution modified to the electrode. As is shown in Fig. S3, 0.5 μM of TDN can provide high signal readout with low background. So 0.5 μM is selected as the optimal TDN concentration for the experiments. In addition, the modification time and salt ion concentration have also been optimized (Fig. S4) The self-assembly process is monitored using a quartz crystal microbalance (QCM), which shows the rapid modification of TDNs on the surface of the electrode. Therefore, we have chosen 1.5 h and 50 mM $MgCl_2$ as the following experimental conditions.

3.3. Quantitative detection of Oct4

Under the optimized conditions, the fabricated sensor has been employed to detect Oct4 at different concentrations. As shown in Fig. 4A, a gradual increase of the peak current is clearly observed along with the increasing concentrations of Oct4. A linear relationship between the Oct4 concentration and the SWV peak current can be established from 0.5–1000 ng/mL (Fig. 4B). The linear regression equation is determined to be $y = 2.32 + 0.01 \times (R^2 = 0.991)$, and the detection limit is 60 pg/mL (Centi et al., 2007). Moreover, to verify the

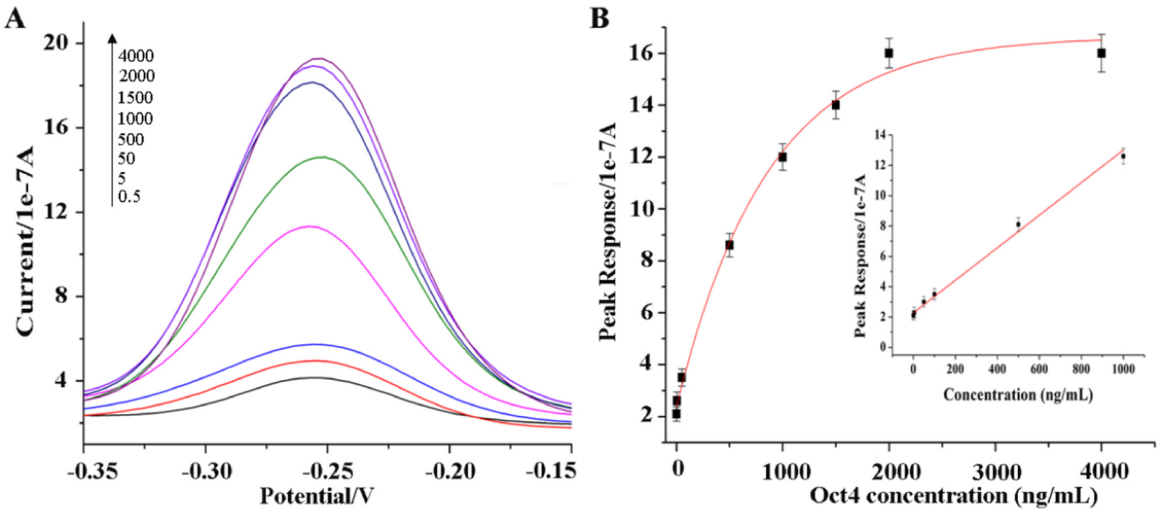

Fig. 4. (A) SWVs corresponding to the detection of different concentrations of Oct4. (B) Calibration curve corresponding to (A). The inserted graph is the linear concentration range. Error bars represent standard deviations of measurements (n = 3).

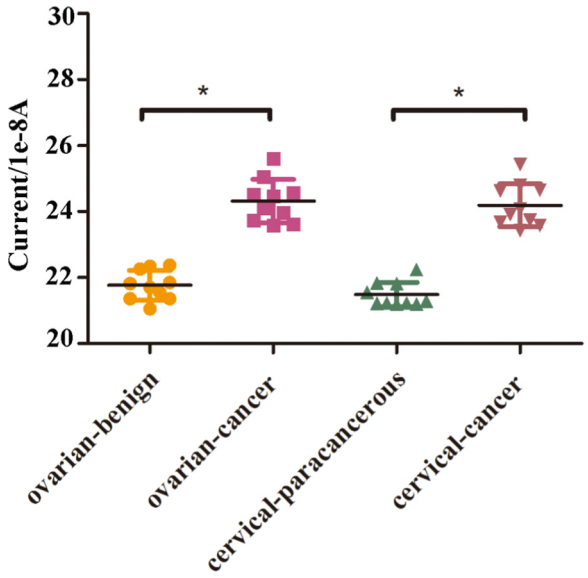

Fig. 5. The distribution of detected Oct4 concentration in human caner tissues and corresponding control tissues (benign or paracancerous). The statistical significances of the observed difference are determined by *t*-test. *: $p < 0.05$.

Table 1
Tissue sample analysis and the comparison with ELISA method.

Sample	ELISA (ng/mL)	Proposed assay (ng/mL)	Relative error (%)
1	8.67	8.9	2.65
2	5.64	5.81	3.01
3	2.23	2.28	2.24
4	4.7	4.85	3.20
5	1.23	1.2	− 2.43

selectivity of this sensor, several control species including BSA and NF-κB were used, and they all produced a background signal only (Fig. S5). Therefore, the results indicate that the selectivity of our sensor is satisfactory.

3.4. Analysis of clinical tissue samples

To further explore the application of the proposed sensor for real sample analysis, the sensor has been used to assay Oct4 in human tissue. As shown in Fig. 5, the peak currents for benign ovarian tissue and cervical paracancerous are rather low, indicating the low expression of Oct4. However, the observed signals for ovarian cancer and cervical cancer tissue apparently increase, suggesting overexpression of Oct4 in cancer tissue. To evaluate the reliability of this sensor, we have compared the assay results of Oct4 using the proposed sensor with the reference values obtained by ELISA in human tissue samples. As shown in Table 1, the estimated values obtained by our method are nearly the same to ELISA, revealing an acceptable accuracy.

4. Conclusions

In summary, we have fabricated an electrochemical sensor for the detection of Oct4 based on our designed TDN. Compared with traditional methods, our sensor is simple and rapid (in less than 30 min). Noteworthy, the sensor has been demonstrated to be able to detect Oct4 in real clinical tissue samples, which may have great potential for the diagnosis of cancer. Certainly, since there is no signal amplification strategy involved in this sensor, more work should be conducted to improve the sensor performance in detection of trace samples in the future. Meanwhile, this work may pave the way for the development of other DNA binding protein analytical systems by just replacing the binding sequence in the TND for the target proteins.

Acknowledgments

This work was supported by the National Natural Science Foundation of China (Grant Nos. 81772593, 81672570).

Declaration of interests

None.

Appendix A. Supporting information

Supplementary data associated with this article can be found in the online version at https://doi.org/10.1016/j.bios.2018.12.029.

References

Atlasi, Y., Mowla, S.J., Ziaee, S.A., Bahrami, A.R., 2007. OCT-4, an embryonic stem cell marker, is highly expressed in bladder cancer. Int J. Cancer 120 (7), 1598–1602.
Centi, S., Tombelli, S., Minunni, M., Mascini, M., 2007. Aptamer-based detection of plasma proteins by an electrochemical assay coupled to magnetic beads. Anal. Chem. 79 (4), 1466–1473.
Comisso, E., Scarola, M., Rosso, M., Piazza, S., Marzinotto, S., Ciani, Y., Orsaria, M., Mariuzzi, L., Schneider, C., Schoeftner, S., Benetti, R., 2017. OCT4 controls mitotic stability and inactivates the RB tumor suppressor pathway to enhance ovarian cancer aggressiveness. Oncogene 36 (30), 4253–4266.
Ge, N., Lin, H.X., Xiao, X.S., Guo, L., Xu, H.M., Wang, X., Jin, T., Cai, X.Y., Liang, Y., Hu, W.H., Kang, T., 2010. Prognostic significance of Oct4 and Sox2 expression in hypopharyngeal squamous cell carcinoma. J. Transl. Med. 8, 94.
Ge, Z., Su, Z., Simmons, C.R., Li, J., Jiang, S., Li, W., Yang, Y., Liu, Y., Chiu, W., Fan, C., Yan, H., 2018. Redox Engineering of cytochrome c using DNA nanostructure-based charged encapsulation and spatial control. ACS Appl. Mater. Interfaces.
Kar, S., Patra, S.K., 2018. Overexpression of OCT4 induced by modulation of histone marks plays crucial role in breast cancer progression. Gene 643, 35–45.
Kim, B.W., Cho, H., Choi, C.H., Ylaya, K., Chung, J.Y., Kim, J.H., Hewitt, S.M., 2015. Clinical significance of OCT4 and SOX2 protein expression in cervical cancer. BMC Cancer 15, 1015.
Kim, K.R., Kim, D.R., Lee, T., Yhee, J.Y., Kim, B.S., Kwon, I.C., Ahn, D.R., 2013. Drug delivery by a self-assembled DNA tetrahedron for overcoming drug resistance in breast cancer cells. Chem. Commun. 49 (20), 2010–2012.
Kim, R.J., Nam, J.S., 2011. OCT4 expression enhances features of cancer stem cells in a mouse model of breast cancer. Lab. Anim. Res. 27 (2), 147–152.
Li, B., Yao, Z., Wan, Y., Lin, D., 2016. Overexpression of OCT4 is associated with gefitinib resistance in non-small cell lung cancer. Oncotarget 7 (47), 77342–77347.
Li, C., Hu, X., Lu, J., Mao, X., Xiang, Y., Shu, Y., Li, G., 2018a. Design of DNA nanostructure-based interfacial probes for the electrochemical detection of nucleic acids directly in whole blood. Chem. Sci. 9 (4), 979–984.
Li, X., Tang, X., Chen, X., Qu, B., Lu, L., 2018b. Label-free and enzyme-free fluorescent isocarbophos aptasensor based on MWCNTs and G-quadruplex. Talanta 188, 232–237.
Li, Z., Li, X., Li, C., Su, Y., Fang, W., Zhong, C., Ji, W., Zhang, Q., Su, C., 2014. Transcription factor OCT4 promotes cell cycle progression by regulating CCND1 expression in esophageal carcinoma. Cancer Lett. 354 (1), 77–86.
Looijenga, L.H., Stoop, H., de Leeuw, H.P., de Gouveia Brazao, C.A., Gillis, A.J., van Roozendaal, K.E., van Zoelen, E.J., Weber, R.F., Wolffenbuttel, K.P., van Dekken, H., Honecker, F., Bokemeyer, C., Perlman, E.J., Schneider, D.T., Kononen, J., Sauter, G., Oosterhuis, J.W., 2003. POU5F1 (OCT3/4) identifies cells with pluripotent potential in human germ cell tumors. Cancer Res. 63 (9), 2244–2250.
Lu, Y., Zhu, H., Shan, H., Lu, J., Chang, X., Li, X., Lu, J., Fan, X., Zhu, S., Wang, Y., Guo, Q., Wang, L., Huang, Y., Zhu, M., Wang, Z., 2013. Knockdown of Oct4 and Nanog expression inhibits the stemness of pancreatic cancer cells. Cancer Lett. 340 (1), 113–123.
Ma, J., Li, C., Tao, Y., Feng, C., Li, G., 2016. Electrochemical detection of Nanog in cell extracts via target-induced resolution of an electrode-bound DNA pseudoknot. Biosens. Bioelectron. 86, 933–938.
Ma, J., Shi, H., Zhang, M., Li, C., Xiang, Y., Liu, P., 2018. A homogeneous, anti-dsDNA antibody-based assay for multicolor detection of cancer stem cell transcription factors. Anal. Chim. Acta 1029, 72–77.
Nie, L., Guo, H., He, Q., Chen, J., Miao, Y., 2007. Enhanced electrochemical detection of DNA hybridization with carbon nanotube modified paste electrode. J. Nanosci. Nanotechnol. 7 (2), 560–564.
Ozhalici-Unal, H., Armitage, B.A., 2009. Fluorescent DNA nanotags based on a self-assembled DNA tetrahedron. ACS Nano 3 (2), 425–433.
Sharma, V.P., Voiculescu, S., Wang, Y., Karagiannis, G.S., Tang, B., Wakefield, L., Entenberg, D., Goswami, S., Oktay, M., Condeelis, J., 2017. Abstract 878: a new SOX2/OCT4 stem cell biosensor reveals the mechanism of cancer stem cell dissemination in human breast cancer. Cancer Res. 77 (13 Supplement) (878-878).
Shen, L., Huang, X., Xie, X., Su, J., Yuan, J., Chen, X., 2014. High expression of SOX2 and

OCT4 indicates radiation resistance and an independent negative prognosis in cervical squamous cell carcinoma. J. Histochem. Cytochem. 62 (7), 499–509.
Wang, Y.D., Cai, N., Wu, X.L., Cao, H.Z., Xie, L.L., Zheng, P.S., 2013. OCT4 promotes tumorigenesis and inhibits apoptosis of cervical cancer cells by miR-125b/BAK1 pathway. Cell Death Dis. 4, e760.
Yan, S., Li, X., Jin, Q., Yuan, J., 2016. MicroRNA-145 sensitizes cervical cancer cells to low-dose irradiation by downregulating OCT4 expression. Exp. Ther. Med. 12 (5), 3130–3136.
Yang, F., Li, Q., Wang, L., Zhang, G.J., Fan, C., 2018. Framework-nucleic-acid-enabled biosensor development. ACS Sens. 3 (5), 903–919.
Yin, X., Li, Y.W., Zhang, B.H., Ren, Z.G., Qiu, S.J., Yi, Y., Fan, J., 2012. Coexpression of stemness factors Oct4 and Nanog predict liver resection. Ann. Surg. Oncol. 19 (9), 2877–2887.
Zhang, R., Wang, X., He, N., 2005. Specific binding of dacarbazine to DNA bases and oligonucleotides based on gold nanoparticles. J. Nanosci. Nanotechnol. 5 (8), 1245–1248.
Zhao, R., Liu, Q., Lou, C., 2018. MicroRNA-299-3p regulates proliferation, migration and invasion of human ovarian cancer cells by modulating the expression of OCT4. Arch. Biochem. Biophys. 651, 21–27.
Zhao, R.C., Zhou, J., Chen, K.F., Gong, J., Liu, J., He, J.Y., Guan, P., Li, B., Qin, Y., 2016. The prognostic value of combination of CD90 and OCT4 for hepatocellular carcinoma after curative resection. Neoplasma 63 (2), 288–298.